Capability Studies of the Heliotron J Soft X-Ray Tomographic Diagnostic*)

Shishir PUROHIT[1)], Yasuhiro SUZUKI[1,2)], Satoshi OHDACHI[1,2)] and Satoshi YAMAMOTO[3)]

[1)]*SOKENDAI, The Graduate University for Advanced Studies, 322-6 Oroshi-cho, Toki, Gifu 509-5292, Japan*
[2)]*National Institute for Fusion Science, 322-6 Oroshi-cho, Toki, Gifu 509-5292, Japan*
[3)]*Institute of Advanced Energy, Kyoto University, Gokasho, Uji, Kyoto 611-0011, Japan*

(Received 28 December 2018 / Accepted 11 February 2019)

Imaging diagnostics offers magnetic free information for the plasma emissions and able to define plasma shape and position, impurity distribution, and magnetohydrodynamics (MHD) instabilities. The tomographic reconstruction is one of the powerful tools to analyze imaging diagnostic data. Tomography is employed for a wide range of plasma studies prominently for the soft X-ray (SX). SX tomography allows access to spatiotemporal transient phenomena resulting from the magnetohydrodynamics (MHD) activities, which are important for plasma confinement. Heliotron J (H-J) is an $L/M = 1/4$ helical axis Heliotron with a low magnetic shear configuration and with a bumpy poloidal plasma shape. An attempt for qualitative evaluation of the tomographic reconstruction capabilities for the Heliotron-J device was made. The tomographic reconstructions were made via Phillips - Tikhonov regularizations from the experimental data set at different locations in the time-space. The results suggests that the diagnostic needs to be improved for a high quality of image reconstruction and possible realization of magnetic axis shift, Shafranov Shift.

Keywords: Heliotron J (H-J), soft X-ray, tomographic reconstruction, Phillips - Tikhonov regularizations and Shafranov shift

DOI: 10.1585/pfr.14.3402056

1. Introduction

Tomographic reconstruction from imaging diagnostics is a widely accepted methodology for transforming the line integrated data into its integrands [1–5], especially for soft X-ray measurements. The line integrated Soft X-ray data (SX) is magnetic free information, and efficiently represents the plasma interior. The reconstruction offers the opportunity to study a range of Magneto-Hydro-Dynamic (MHD) equilibrium and stability issues including magnetic islands [6, 7], Shafranov shift, and others.

Different mode structure appears in the plasma for a variety of plasma operation regime. The growth trajectory for these mode structures is important to know as it greatly influences the plasma stability [6]. Along with that, the Shafranov shift, the shift of the magnetic axis due to the Pfirsch-Schluter current, degrades energetic particle confinement as the magnetic axis moves outwards. This is a serious threat to the MHD equilibrium and stability [8]. This paper presents soft X-ray tomographic reconstruction for the NBI heated Heliotron J plasma [9, 10]. One of the main objectives is to generate the tomographic images to understand the equilibrium plasma and eventually lead to the realization of the Shafranov shift [11]. The second objective is to visualize different mode structures possibly present in NBI heated Heliotron J plasma [12, 13]. Section II describes the Heliotron J device along with the soft X-ray tomography diagnostic. The following section III elaborates the tomographic reconstruction techniques. The results are discussed in section IV.

2. Heliotron J (H-J)

The Heliotron J (H-J) is a mid-sized helical axis heliotron device, aimed at a high-level of compatibility between good particle confinement and MHD stability. H-J also addresses the non-symmetric quasi - isodynamic (quasi-omnigenous) optimization in the helical-axis geometry. The Heliotron J device is configured as $L/M = 1/4$ helical coil with pitch modulation of - 0.4, highly negative pitch modulation ensures good particle confinement and edge magnetic well. Two dedicated toroidal coils excite the toroidal field on magnetic axis to $\boldsymbol{B}_{t0} \sim 1T$ and control the bumpiness in the toroidal field. The poloidal coils, inner vertical coil (IV), auxiliary mid-vertical coil (AV), and outer main vertical coil (V) provide multipole field components as well as being responsible for maintaining the plasma position, magnetic-well depth, and bumpiness. These coils significantly contribute when the beta is increasing by preventing the breakup of the outer magnetic surfaces [9]. Table 1 formally defines the Heliotron J device in terms of plasma and device parameters.

As shown in table 1 H-J is equipped with a range of

author's e-mail: shishir.purohit@nifs.ac.jp

*) This article is based on the presentation at the 27th International Toki Conference (ITC27) & the 13th Asia Pacific Plasma Theory Conference (APPTC2018).

Table 1 Overview of Heliotron J device.

Coils for magnetic configuration	• Single helical coil (l =1) • Two kinds of toroidal coils • Inner vertical coil • Outer vertical coil	
Major radius (R)	m	1.2
Minor radius (a)	m	<0.25
Toroidal period	N	4
Toroidal field (B)	T	<1.5
ECH Power P_{ECH}	kW	<500
NBI Power P_{NBI}	kW	<700 x 2 (co. and ctr.)
ICRF Power P_{ICRF}	kW	<2500
NBI Energy E_{NBI}	keV	<30
Working gas		D
Rotational transform		0.4~0.7
*Transport and flow	Nd: YAG-TS, CXRS, ECE, Hα array, FIR, Reflectometer	
*Turbulence	LP, BES, Fast camera	
*MHD equilibrium and stability	MP, SXCT, BES, ECE, Reflectometer, Saddle loop (SL), Magnetics	
*Energetic particle	NPA(E//B), DLP, Faraday-cup LIP (FLIP)	

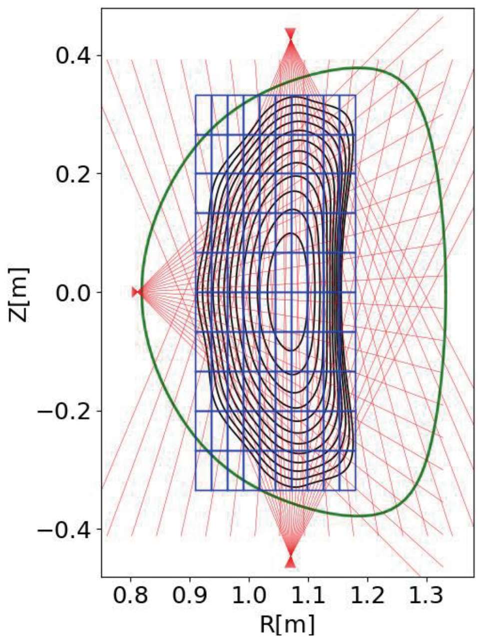

Fig. 1 The viewing geometry for current SX design at H-J. Pixel grid (blue) shows the reconstruction area along with the vacuum vessel boundary (green). The LOS of individual detector red lines (red) views the plasma completely.

diagnostics*, facilitating the studies of different aspects of H-J plasma. One important diagnostic is Soft X-ray tomographic (SXT) system. SXT system is a triad of SX detector arrays with a field of view (FOV) covering the plasma cross-section, as shown in Fig. 1. The SX arrays are installed at the top, at the bottom, and at radial ports to constitute the complete viewing geometry. The FOV is governed by a rectangular pinhole with a submillimeter poloidal opening. The SXT system is installed at φ = 45° toroidal angle. The detector array of SXT is AXUV20ELG detector and has 20 detecting elements within. Thus, the system effectively offers a total of 60 lines of sight (LOS) for the SX measurements of H-J plasma (20 × 3 = 60). An aluminum filter is applied to these detectors for the low energy photons cut-off at ~ 0.75 keV [14]. The detector arrays are connected with an efficient data acquisition system which converts the SX energy deposited in the detector into voltages as a function of time with an acquiring rate of 10 kHz.

3. Tomographic Reconstruction

Soft X-ray tomographic (SXT) reconstructions for H-J are carried out by discreet pixel method. The poloidal cross-section of the H-J plasma is divided into small subregions, referred to as pixels, within which soft X-ray emissions are assumed to be constant. A rectangular pixel shape is considered in the work presented in this paper. The size of the pixel is an important parameter which is directly associated with the resolution of the reconstructed image [15, 16]. An example pixel grid of 10 × 10 (total 100 pixels) is shown in Fig. 1, in blue color.

The line integrated SX signal at a given time is defined in terms of pixel and local emissivity by equation 1.

$$b_i = \sum_i A_{ij} E_j. \tag{1}$$

Where b_i is the line integrated SX for the i^{th} detector, A_{ij} is the contribution matrix element and represents the emission contribution for i^{th} LOS of j^{th} pixel and E_j is the local SX emission of the j^{th} pixel. The plasma tomography is a limited angle tomography, therefore, the contribution estimation is available for a limited number of locations resulting reconstruction problem to be ill-posed problem [1, 4, 17] and the direct inversion of contribution matrix is not possible.

The tomographic reconstruction problem is solved via regularization assisted Least Square Error fitting (LSEF). The regularized tomographic problem is expressed by equation 2.

$$j(E) = \gamma PF(E) + \|b - AE\|^2. \tag{2}$$

Where the γ is the regularization parameter which decides the amount of the regularization and is calculated by Generalized Cross Validation (GCV) [18] method. The $PF(E)$ is the objective or penalty functional, with E is in discrete form. The Phillips-Tikhonov (PT) regularizations are employed here in this work and the penalty function is defined by equation 3. The PT regularization contains a Laplacian filter which introduces the smoothness in the final result.

$$PF(E) = \iint |\nabla^2 E(x, y)|^2 dxdy. \tag{3}$$

Due to the nature of the PT penalty function, the emissivity can be analytically calculated by equation 4 considering the SVD.

$$E(\gamma) = \frac{1}{M} \sum_{j=1}^{M} \frac{\sigma_j}{\sigma_j^2 + M\gamma} v'_{kj} (U^T b)_j. \tag{4}$$

Where v'_{kj} is the element of $V` = C^{-1}V$, and V is determined from the SVD of $(AC^{-1}) = U\Sigma V^T$. The σ is the singular values obtained from the SVD. The k stands for the pixel [19, 20]. Equation 4 gives freedom on singular values of contribution matrix which eventually improves the reconstruction quality.

4. Results and Discussion

A typical Heliotron J discharge is shown in Fig. 2, for which the reconstruction is performed. The Fig.2 represents time evolution of frequency spectrum of magnetic fluctuations obtained from the magnetic probe (MP1) (a), stored plasma energy, ECH, and two NBIs (b), line-averaged electron density and H_α (c), magnetic fluctuation amplitude for MP1 and plasma current (d), Carbon (III) and Oxygen (V) impurity (e), and SX signal bottom array (f) for H-J discharge No. #63300. Discharge is initiated with the introduction of ECH (0.17 s) which can be seen as in the spike increase in the H_α, n_e signal. The frequency analysis (a) shows that high-frequency fluctuations (f_{eq} > 20 kHz) appears from 0.19 s. These fluctuations start reducing with the increase in the density and plasma internal energy, and eventually disappear by 0.22 s. Such fluctuations are most likely associated with the energetic ion-driven (EID) global Alfvén eigenmodes. The two NBIs are employed ~ 0.185 s, resulting in causing the plasma density to rise ~ 0.20 s. As density starts increasing (0.20 s) the soft X-ray signal improves and peaks at ~ 0.25 s.

The tomographic reconstructions are made at two different locations in time-space, first at 0.23 s where the soft X-ray signal is quite low and second at 0.25 s where the soft X-ray signal strength is considerably high, higher beta value. Referring to Fig. 2 (a), Energetic ion driven fluctuations have frequencies greater than 20 kHz. Considering the fact that the SX diagnostic data acquiring rate is 10 kHz, the recovery of these mode structures are not possible with the current data set.

The Soft X-ray signals obtained from the experiments consist of high-frequency noise, and a filtering is required for quality tomographic reconstruction. The Fast-Fourier transform filters the SX signals. The filtered signals can be seen in Fig. 3, where the raw signal (blue) from the central channel of the lower SX array and filtered signal (orange).

The tomographic reconstruction for H-J plasma considering the methodology discussed in section 3 is shown in Fig. 4 for time 0.23 s (top row) and 0.25 s (lower row) with different pixel density (right to left 10 × 10, 20 × 20, and 30 × 30). The image quality improves with the increases in the pixel density. The PT regularizations offers strong smoothening effect via Laplacian operator. Therefore, higher pixel density holds more smoothing and does not provide an appropriate realization of plasma physical image.

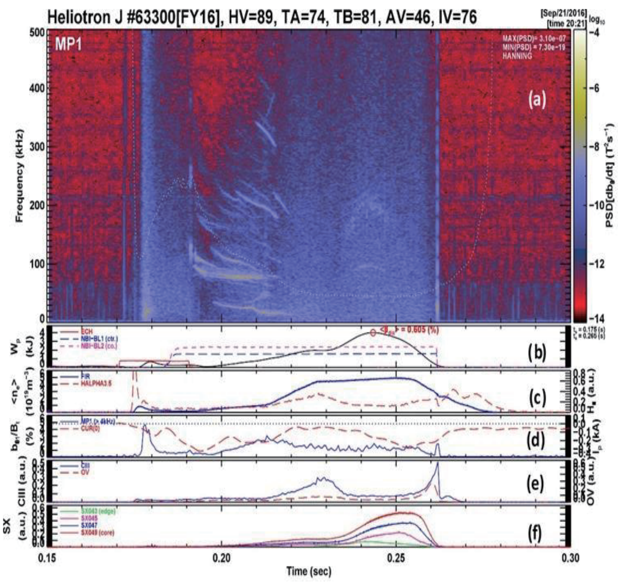

Fig. 2 The Heliotron J typical discharge #63300.

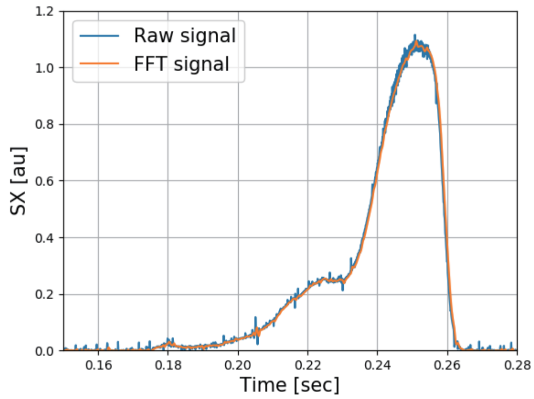

Fig. 3 Raw signal (blue) of central channel of lower detector array and FFT filtered SX signal (orange).

The recovery of the plasma emission profile and possible sensing of magnetic axis shift, Shafranov shift are some the important MHD information which can be estimated by tomographic reconstructions of equilibrium H-J plasma. The soft X-ray tomographic diagnostic at H-J is having 60 lines of sight which unfortunately allows only lower pixel density, bigger pixel size. The tomographic images made with bigger pixel size will not be very sensitive towards the local fluctuations in the plasma emission profile. Such images lacks the capability to reproducing the actually emission profile and may not even sense the shafranov shift, in other words poor resolution. Increasing the lines of sights will improve this situation and add

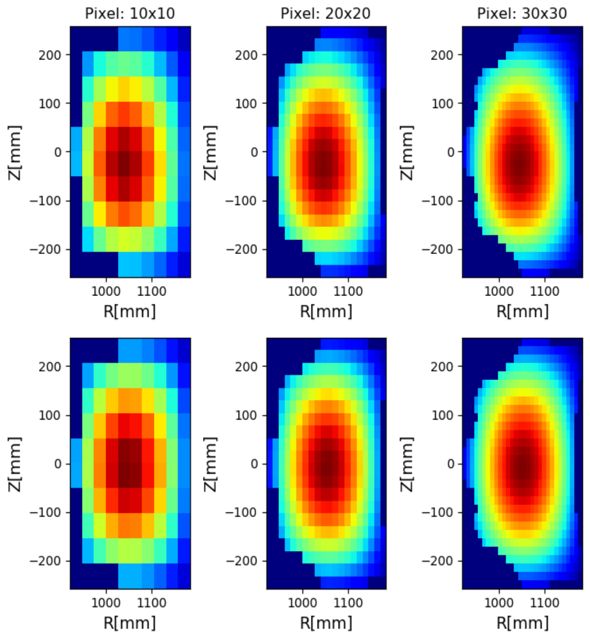

Fig. 4 Reconstructed images at time locations 0.23 s (I row) and 0.25 s (II row) at pixel density 10 × 10 (I column), 20 × 20 (II column), and 30 × 30 (III column).

to the reliability of the reconstructed tomographic image. Simulations studies with modified design of H-J, which includes the increase in the number of arrays in the poloidal plane, shows the improvement in the image quality of the reconstruction [21].

5. Summary

The soft X-ray tomographic reconstructions from Phillips-Tikhonov regularization assisted least-square error fitting for Heliotron J plasma discharge were attempted. The reconstructed images were produced with different pixel densities at different time locations. The increase in the pixel density showed improving in the reconstructed image quality due to strong laplacian smoothening effect. Unfortunately due to the less number of lines of sight the recovery of the soft X-ray emission profile and the possible realization of shafranov shift was not achieved within the present resolution of the tomography system. The improvement in the diagnostic design is required in order to have a better realization of emission profile.

[1] L.C. Ingesson, B. Alper, B.J. Peterson and J.C. Vallet, Fusion Sci. Technol. **53**, 528 (2008).

[2] D. Lluveras Núñez, M.Á. Molero-Armenta, M.Á.G. Izquierdo, M.G. Hernández and J.J. Anaya Velayos, Sensors (Basel) **17**, 1085 (2017).

[3] T. Ming, S. Ohdachi and Y. Suzuki, Plasma Sci. Technol. **15**, 1178 (2013).

[4] N. Iwama and S. Takamura, Med. Imaging Technol. (In Japanese) **13**, 132 (1995).

[5] R.S. Granetz and P. Smeulders, Nucl. Fusion **28**, 457 (1988).

[6] A. Weller, J. Geiger, M. Zarnstorff, E. Sallander, S. Klose, A. Werner, J. Baldzuhn, R. Brakel, R. Burhenn, H. Ehmler, F. Gadelmeier, L. Giannone, D. Hartmann, R. Jaenicke, J. Knauer, H.P. Laqua, C. Nührenberg, E. Pasch, N. Rust *et al.*, "Investigation of the β-Limit in the W7-AS Stellarator", in: 19th Fusion Energy Conf. 14-19 October, Lyon, Fr. (2001), p.EX/S3-1.

[7] Y. Nagayama, J. Appl. Phys. **62**, 2702 (1987).

[8] S. Murakami, M. Okamoto, N. Nakajima, M. Ohnishi and H. Okada, Nucl. Fusion **34**, 913 (1994).

[9] T. Obiki, F. Sano, M. Wakatani, K. Kondo, T. Mizuuchi, K. Hanatani, Y. Nakamura, K. Nagasaki, H. Okada, M. Nakasuga, S. Besshou and M. Yokoyama, Plasma Phys. Control. Fusion **42**, 1151 (2000).

[10] M. Wakatani, Y. Nakamura, K. Kondo, M. Nakasuga, S. Besshou, T. Obiki, F. Sano, K. Hanatani, T. Mizuuchi, H. Okada, K. Nagasaki, N. Inoue and M. Yokoyama, Nucl. Fusion **40**, 569 (2000).

[11] V.D. Shafranov, Sov. At. Energy **13**, 1149 (1963).

[12] S. Yamamoto, K. Nagasaki, S. Kobayashi, K. Nagaoka, A. Cappa, H. Okada, T. Minami, S. Kado, S. Ohshima, S. Konoshima, Y. Nakamura, A. Ishizawa, G.M. Weir, N. Kenmochi, Y. Ohtani, X. Lu, Y. Tawada, D. Kokubu and T. Mizuuchi, Nucl. Fusion **57**, 126065 (2017).

[13] S. Yamamoto, K. Nagasaki, Y. Suzuki, T. Mizuuchi, H. Okada, S. Kobayashi, B. Blackwell, K. Kondo, G. Motojima, N. Nakajima, Y. Nakamura, C. Nührenberg, Y. Torii, S. Watanabe and F. Sano, Fusion Sci. Technol. **51**, 92 (2007).

[14] K. Nishikawa, S. Yamamoto, T. Mizuuchi and K. Nagasaki, "Studies of Magnetohydrodynamics Equilibrium and Stability by Using Soft X-ray CT in High Density Plasmas of Heliotron J", in: Plasma Conf. 18-21 November, Niigata, Japan (2014), p.19PA-027.

[15] M. Al-Frejat and M. HjoujBtoush, Int. J. Adv. Comput. Sci. Appl. **7**, 476 (2016).

[16] M. Yang, X. Wang, Y. Liu, F. Men, X. Li, W. Liu and D. Wei, Chinese Phys. C **38**, 046202 (2013).

[17] N. Iwama and S. Ohdachi, J. Plasma Fusion Res. **82**, 399 (2006).

[18] G.H. Golub, M. Heath and G. Wahba, Technometrics **21**, 215 (1979).

[19] N. Iwama, H. Yoshida, H. Takimoto, Y. Shen, S. Takamura and T. Tsukishima, Appl. Phys. Lett. **54**, 502 (1989).

[20] S. Ohdachi, K. Toi, G. Fuchs, the TEXTOR Team and the LHD Experimental Group, Plasma Sci. Technol. **8**, 45 (2006).

[21] S. Purohit, Y. Suzuki, S. Ohdachi and S. Yamamoto, Rev. Sci. Instrum, **89**, 10 (2018).